How cholesterol stiffens unsaturated lipid membranes

Saptarshi Chakraborty[a,b], Milka Doktorova[c], Trivikram R. Molugu[d], Frederick A. Heberle[e,f], Haden L. Scott[g,h], Boris Dzikovski[i], Michihiro Nagao[j,k,l], Laura-Roxana Stingaciu[e], Robert F. Standaert[m], Francisco N. Barrera[g], John Katsaras[e,n], George Khelashvili[o,p], Michael F. Brown[d,1], and Rana Ashkar[a,b,1]

[a]Department of Physics, Virginia Tech, Blacksburg, VA 24061; [b]Center for Soft Matter and Biological Physics, Virginia Tech, Blacksburg, VA 24061; [c]Department of Integrative Biology and Pharmacology, University of Texas Health Science Center, Houston, TX 77030; [d]Department of Chemistry and Biochemistry, University of Arizona, Tucson, AZ 85721; [e]Neutron Scattering Division, Oak Ridge National Laboratory, Oak Ridge, TN 37831; [f]Bredesen Center, University of Tennessee, Knoxville, TN 37996; [g]Department of Biochemistry and Cellular and Molecular Biology, University of Tennessee, Knoxville, TN 37996; [h]Center for Environmental Biotechnology, University of Tennessee, Knoxville, TN 37920; [i]ACERT, National Biomedical Center for Advanced ESR Technology, Department of Chemistry and Chemical Biology, Cornell University, Ithaca, NY 14853; [j]Center for Neutron Research, National Institute of Standards and Technology, Gaithersburg, MD 20899; [k]Department of Physics and Astronomy, University of Delaware, Newark, DE 19716; [l]Center for Exploration of Energy and Matter, Department of Physics, Indiana University, Bloomington, IN 47408; [m]Biosciences Division, Oak Ridge National Laboratory, Oak Ridge, TN 37831; [n]Shull Wollan Center, Oak Ridge National Laboratory, Oak Ridge, TN 37831; [o]Department of Physiology and Biophysics, Weill Cornell Medical College, New York, NY 10065; and [p]Institute of Computational Biomedicine, Weill Cornell Medical College, New York, NY 10065

Edited by Cyrus R. Safinya, University of California, Santa Barbara, CA, and accepted by Editorial Board Member Lia Addadi July 14, 2020 (received for review March 13, 2020)

Cholesterol is an integral component of eukaryotic cell membranes and a key molecule in controlling membrane fluidity, organization, and other physicochemical parameters. It also plays a regulatory function in antibiotic drug resistance and the immune response of cells against viruses, by stabilizing the membrane against structural damage. While it is well understood that, structurally, cholesterol exhibits a densification effect on fluid lipid membranes, its effects on membrane bending rigidity are assumed to be nonuniversal; i.e., cholesterol stiffens saturated lipid membranes, but has no stiffening effect on membranes populated by unsaturated lipids, such as 1,2-dioleoyl-*sn*-glycero-3-phosphocholine (DOPC). This observation presents a clear challenge to structure–property relationships and to our understanding of cholesterol-mediated biological functions. Here, using a comprehensive approach—combining neutron spin-echo (NSE) spectroscopy, solid-state deuterium NMR (^{2}H NMR) spectroscopy, and molecular dynamics (MD) simulations—we report that cholesterol locally increases the bending rigidity of DOPC membranes, similar to saturated membranes, by increasing the bilayer's packing density. All three techniques, inherently sensitive to mesoscale bending fluctuations, show up to a threefold increase in effective bending rigidity with increasing cholesterol content approaching a mole fraction of 50%. Our observations are in good agreement with the known effects of cholesterol on the area-compressibility modulus and membrane structure, reaffirming membrane structure–property relationships. The current findings point to a scale-dependent manifestation of membrane properties, highlighting the need to reassess cholesterol's role in controlling membrane bending rigidity over mesoscopic length and time scales of important biological functions, such as viral budding and lipid–protein interactions.

area compressibility | membrane viscosity | deuterium NMR | neutron spin echo | molecular dynamics simulations

Lipid bilayers, the underlying scaffold of cellular membranes, consist of a rich mixture of lipids and sterols. Among sterols, cholesterol (Chol) is uniquely linked to cell evolution (1)—it is universally absent in prokaryotic membranes and is present in differing amounts in eukaryotic membranes, ranging from a mole fraction (mol%) of <5 mol% in mitochondrial membranes up to 40 mol% in plasma membranes (2). Chol plays an essential regulatory function in many biomembrane processes (3), including passive permeation (4), protein and enzyme activity (5, 6), and the formation of raft-like domains (7) associated with cell signaling and intracellular trafficking. It is also directly implicated in viral infections (8), including influenza (9), HIV (10), and, recently, coronavirus (11). Deviations from normal Chol levels disrupt membrane functions and result in impaired immune responses and numerous other health anomalies (12–14). Given Chol's biological importance, studies detailing its effects on membrane mechanics have justifiably taken center stage in recent years (15–17). Various techniques (18, 19), including flicker spectroscopy, micropipette aspiration, electrodeformation, and NMR spectroscopy, have been used to examine the interdependence of structure, mechanics, and dynamics proposed by Helfrich in the early 1970s (20, 21). While early studies performed on single-component lipid membranes exhibited the expected dependence of the bending rigidity as a function of membrane thickness and packing density (22), later studies on Chol-containing membranes showed striking deviations from this behavior, which, surprisingly, depended on the level of lipid acyl-chain unsaturation (23, 24). Given the lipid diversity in cell membranes and the significance of mesoscale bending energetics in viral budding (25) and membrane–protein interactions (26), it is

Significance

Cholesterol regulates critical cell functions, including lysis, viral budding, and antibiotic resistance, by modifying the bending rigidity of cell membranes; i.e., the ability of membranes to bend or withstand mechanical stresses. A molecular-level understanding of these functions requires knowledge of how cholesterol modifies membrane mechanics over relevant length and time scales. Currently, it is widely accepted that cholesterol has no effect on the mechanical properties of unsaturated lipid membranes, implying that viruses, for example, can bud from regions enriched in (poly)unsaturated lipids. Our observations that cholesterol causes local stiffening in DOPC membranes indicate that a reassessment of existing concepts is necessary. These findings have far-reaching implications in understanding cholesterol's role in biology and its applications in bioengineering and drug design.

Author contributions: R.A. designed overall research project; M.F.B. designed NMR studies; S.C. and R.A. collected and analyzed small-angle neutron scattering and neutron spin-echo data; S.C. and T.R.M. collected and analyzed NMR data; M.D. and G.K. performed molecular dynamics simulations; F.A.H., H.L.S., F.N.B., and J.K. collected and analyzed small-angle X-ray scattering data; B.D. collected and analyzed electron spin resonance data; R.F.S. synthesized deuterated lipids; M.N. and L.-R.S. assisted with neutron spin-echo studies; S.C., M.D., T.R.M., F.A.H., H.L.S., B.D., M.N., L.-R.S., R.F.S., F.N.B., J.K., G.K., M.F.B., and R.A. discussed and reviewed the results; and R.A. wrote the manuscript with input from all authors.

The authors declare no competing interest.

This article is a PNAS Direct Submission. C.R.S. is a guest editor invited by the Editorial Board.

[1]To whom correspondence may be addressed. Email: ashkar@vt.edu or mfbrown@u.arizona.edu.

This article contains supporting information online at https://www.pnas.org/lookup/suppl/doi:10.1073/pnas.2004807117/-/DCSupplemental.

First published August 25, 2020.

incumbent to elucidate whether the lack of Chol-induced stiffening in unsaturated membranes is manifested on biologically relevant length and time scales.

Here, we report experimental mesoscale studies of the effects of Chol on bending dynamics of unsaturated lipid membranes composed of 1,2,-dioleoyl-*sn*-glycero-3-phosphocholine (DOPC; also abbreviated as diC18:1PC). The experiments are supplemented by real-space fluctuation (RSF) analysis of atomistic molecular dynamics (MD) simulations (27, 28). Collective dynamics of DOPC–Chol membranes were measured by using neutron spin-echo (NSE) spectroscopy on unilamellar vesicles and solid-state deuterium (^{2}H) NMR spectroscopy on multilamellar dispersions. The NSE studies enabled calculations of the effective membrane bending rigidity modulus, κ (29, 30), and revealed a consistent increase in κ with increasing Chol content, in excellent agreement with RSF-MD simulation results. The solid-state ^{2}H NMR measurements yielded a similar relative increase in the bending modulus, as observed by NSE, confirming the membrane-stiffening effect of Chol over comparable length and time scales. The remarkable agreement between NSE spectroscopy, solid-state ^{2}H NMR spectroscopy, and RSF-MD simulations—all of which access mesoscale bending fluctuations—points to a membrane-stiffening effect of Chol over short length and time scales. This result differs from previous experiments reporting on microscopic scales, where no mechanical effect due to Chol was detected in DOPC membranes (23, 24). Importantly, the changes in bending rigidity are in accord with Chol-induced membrane structural changes obtained from the MD simulations and confirmed by small-angle X-ray/neutron

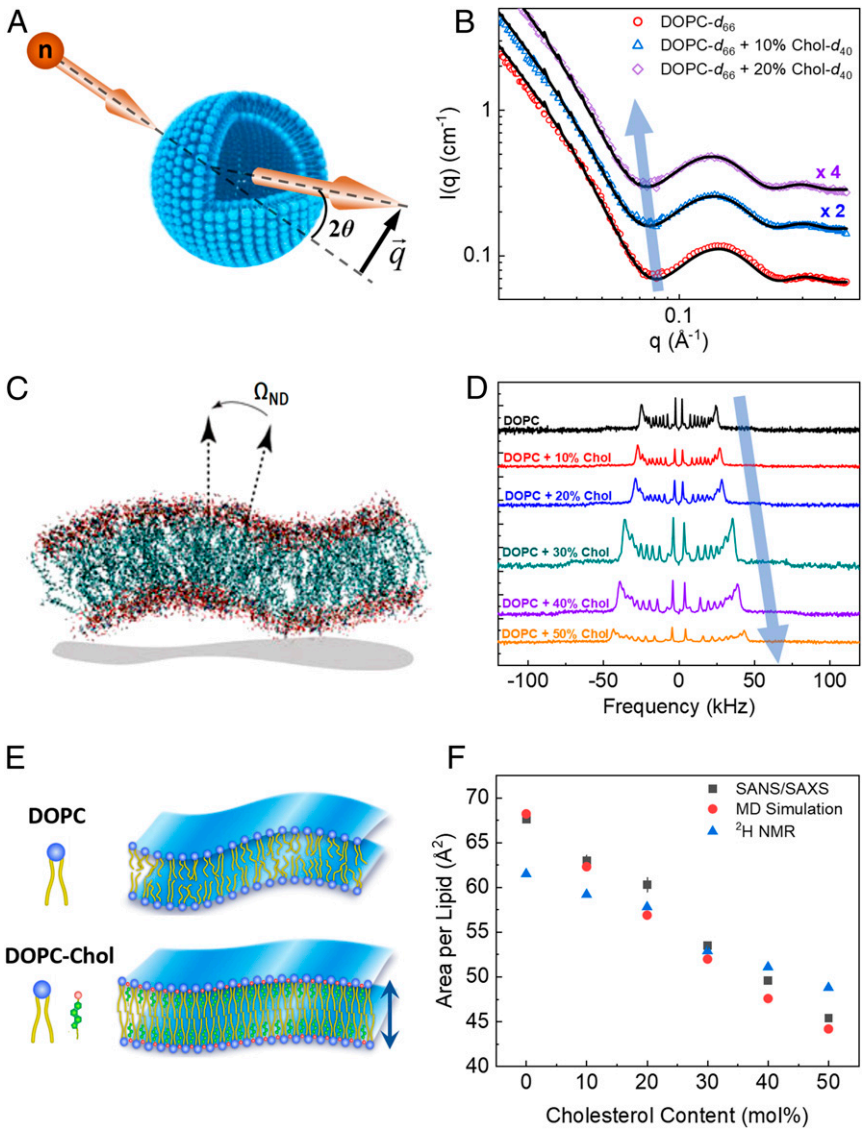

Fig. 1. Structural measurements indicate Chol-induced increase in membrane thickness and lipid packing. (*A*) Schematic of neutron scattering from lipid vesicles with a scattering angle 2θ and wavevector transfer $\vec{q}$. (*B*) SANS data on vesicles of tail-perdeuterated DOPC–Chol indicate membrane thickening with increasing Chol content, indicated by decreasing q values of the scattering intensity minimum. The lines are fits to the data, as described in *SI Appendix*. (*C*) Simulation snapshot of a lipid bilayer depicting membrane fluctuations and the geometry of director vectors used in ^{2}H NMR data analysis. (*D*) Solid-state ^{2}H NMR spectra show increased Chol-induced acyl-chain ordering in multilamellar dispersion of DOPC, indicated by the increasing quadrupolar splitting of the POPC-d_{31} probe with increasing mol% Chol. (*E*) Illustration of the structural effects of Chol on DOPC membranes, i.e., increased membrane thickness and lipid packing. The latter is demonstrated in *F*, where the average area per lipid shows clear decrease with increasing Chol content, as obtained from joint SANS/SAXS data analysis, solid-state ^{2}H NMR lineshape analysis, and RSF-MD simulations. Error bars represent ±1 SD in all figures and may be smaller than the symbol size.

scattering (SAXS/SANS), solid-state ^{2}H NMR lineshape analysis, and electron spin resonance (ESR). Finally, the area compressibility moduli, K_A, of DOPC–Chol membranes were calculated by using the modified polymer-brush model validated by RSF-MD simulations. These K_A values were used in the analysis of NSE data (31) of tail-perdeuterated DOPC–Chol membranes to estimate the membrane viscosity at various Chol concentrations. Our findings reaffirm membrane structure–property relationships encompassed by the polymer-brush model (32) and indicate length-and time-scale dependence of Chol-induced mechanical properties in DOPC membranes. These observations impel a reassessment of the functional role of Chol in mesoscopic membrane functions, such as viral budding and lipid–protein interactions.

Results

Structural Effects of Chol on DOPC Membranes. Chol-induced structural changes in unilamellar vesicles of DOPC membranes were investigated by using SAXS/SANS (Fig. 1 *A* and *B* and *SI Appendix*, Fig. S1). Joint analysis of the SAXS and SANS data yielded the total membrane thickness (D_B), the hydrocarbon thickness ($2D_C$), phosphate-to-phosphate (p-p) thickness, and the average area per lipid (A_L) (*SI Appendix*, Tables S1 and S2). The results showed a monotonic increase in the bilayer thickness (*SI Appendix*, Fig. S2) with increasing amounts of Chol, in agreement with the accepted picture of Chol residing in an upright position among the hydrocarbon chains (33) beneath the lipid head groups (33), manifesting in membrane thickening (34). The p-p thickness obtained from fits to the SAXS data yielded values between 35.2 Å for DOPC membranes and 39.9 Å for DOPC–Chol membranes at 50 mol% Chol (*SI Appendix*, Table S2), in excellent agreement with X-ray diffraction studies of multilamellar stacks and SAXS studies of DOPC–Chol unilamellar vesicles (35, 36). This increase in p-p thickness, with increasing mol% Chol, was accompanied by a decrease in the area per lipid (A_L) (Fig. 1*F*), in good agreement with published reports (36).

Similar results were obtained from solid-state ^{2}H NMR equilibrium lineshape measurements on multilamellar stacks of DOPC–Chol membranes doped with 10 mol% proxy lipid, 1-palmitoyl-2-oleoyl-*sn*-glycero-3-phosphocholine (POPC)-d_{31} (Fig. 1*D*). In these experiments, we measured the residual quadrupolar coupling of ^{2}H nuclei (spin = 1) with the C–^{2}H electric-field gradient. The de-Paked (37, 38) signal showed an increase in quadrupolar splitting with increasing Chol content, indicating greater acyl chain ordering (see *SI Appendix*, Fig. S3 for peak assignments). Analysis of the ^{2}H NMR equilibrium lineshapes, following the statistical mean-torque model (39), showed a clear Chol-induced thickening of DOPC membranes (*SI Appendix*, Fig. S4 and Table S3) and a concomitant decrease in the area per lipid (Fig. 1*F*), supporting the observations from scattering experiments.

To further elucidate the effects of Chol on bilayer structure, we performed all-atom MD simulations on model DOPC–Chol membranes. An earlier study (28) had reported simulation results from DOPC–Chol membranes containing (0, 10, 20, and 40) mol% Chol, which we supplemented with MD simulations of DOPC containing (30 and 50) mol% Chol. Analysis of the various structural parameters from the simulations showed that the average area per molecule decreased steadily from ∼68 Å^2 at 0 mol% Chol to ∼44 Å^2 at 50 mol% Chol (Fig. 1*F*). Similarly, the partial area of DOPC also decreased, consistent with results from a previous report (34). As expected, membrane thickness and acyl-chain order parameters (*SI Appendix*, Fig. S5) increased as well, emphasizing the extent of structural changes induced by Chol in DOPC membranes. These results are also in excellent agreement with order-parameter measurements by ESR (*SI Appendix*, Fig. S5). Put together, the structural parameters of DOPC–Chol membranes obtained from SANS/SAXS, solid-state ^{2}H NMR, and ESR closely replicate the results from MD simulations (Fig. 1*F*). These observations elucidate Chol-induced ordering of DOPC acyl chains, causing the membrane to thicken and the lipids to pack more tightly.

NSE Spectroscopy Reveals Chol-Induced Stiffening of DOPC Membranes. Our NSE spectroscopy measurements were performed on unilamellar vesicles of DOPC–Chol membranes in deuterated buffer to examine changes in the membrane bending rigidity as a function of increasing Chol content. NSE directly probes membrane dynamics over length scales ranging from tens to hundreds of Angstroms and time scales from 10 ps to 100 ns. For lipid membranes, the dynamics in this spatiotemporal range are mainly collective thermal fluctuations in the form of bending- and thickness-fluctuation modes (30). To separate the two fluctuation modes, we employed different lipid-deuteration schemes, as described hereafter. Bending fluctuations were selectively measured by using protiated forms of lipid vesicles and by tuning the NSE spectrometer to length scales that are intermediate between the bilayer thickness and the vesicle size. The NSE dynamic structure factor (Fig. 2*A* and *SI Appendix*, Fig. S6) is described by a stretched-exponential function: $I(q,t)/I(q,0) = \exp[-(\Gamma_{bend}(q)t)^{2/3}]$, where $\Gamma_{bend}(q)$ is the decay rate of the bending fluctuations. Our measurements showed that the dynamic structure factor at all wave vectors, q, decays more slowly for DOPC–Chol membranes compared to DOPC membranes (Fig. 2*A*). This model-free observation is a clear indication of a Chol-induced slowdown in collective membrane dynamics over the accessed NSE length and time scales. Quantitative assessment of changes in membrane stiffness associated with the observed reduction in bending dynamics was obtained from the analysis of $\Gamma_{bend}(q)$, which showed the typical q^3 dependence for thermally undulating elastic thin sheets predicted by Zilman and Granek (40) (Fig. 2*B*). Further theoretical refinements by Watson and Brown (41), following the Seifert–Langer model (42), which takes into account the nature of the finite thickness of coupled monolayers, yielded a renormalized bending rigidity $\tilde{\kappa} = \kappa + 2h^2k_m$, where h is the height of the neutral surface from the midplane and k_m is the monolayer area compressibility modulus.

Using this refinement and defining the neutral plane to be at the interface between the hydrophilic headgroups and the hydrophobic tails results in a modified expression of the Zilman–Granek decay rates, $\Gamma_{bend}(q)$, namely (31):

$$\Gamma_{bend}(q) = 0.0069\frac{k_BT}{\eta_{sol}}\sqrt{\frac{k_BT}{\kappa}}q^3. \quad [1]$$

Here, k_BT is the thermal energy, η_{sol} is the solvent (i.e., D_2O or ^2H_2O) viscosity, and the wavevector transfer, q, is given by the neutron wavelength, λ, and the scattering angle, 2θ, as $q = 4\pi\sin\theta/\lambda$. Fits of $\Gamma_{bend}(q)$ to Eq. **1** enabled calculations of the effective bending rigidity modulus, κ, for DOPC–Chol membranes at different mol% Chol—i.e., 0 to 50 mol%. Our results indicate a noticeable increase in κ with increasing Chol content (*SI Appendix*, Table S4). Specifically, κ for DOPC membranes (100-nm-diameter vesicles) was found to be $(19.05 \pm 0.65)k_BT$ or $(7.8 \pm 0.3) \times 10^{-20}$ J, in close agreement with previously reported values obtained from diffuse X-ray scattering ($\kappa \approx 8 \times 10^{-20}$ J) (23) and electrodeformation ($\kappa \approx 9 \times 10^{-20}$ J) (24) measurements. On the other hand, measurements with 10 mol% and 20 mol% Chol resulted in bending rigidity values of $(22.46 \pm 1.77)k_BT$ and $(30.34 \pm 2.47)k_BT$, respectively, indicating a noticeable increase in κ. Additional measurements on 50-nm-diameter vesicles with an extended Chol range showed similar trends in the relative bending-rigidity modulus, κ/κ_0 (where κ_0 is the bending modulus of DOPC), up to an ∼3-fold increase at 50 mol% Chol (*SI Appendix*, Table S4). As shown in Fig. 2*B*, the slope for $\Gamma_{bend}(q)$ of DOPC membranes is greater than DOPC–Chol membranes.

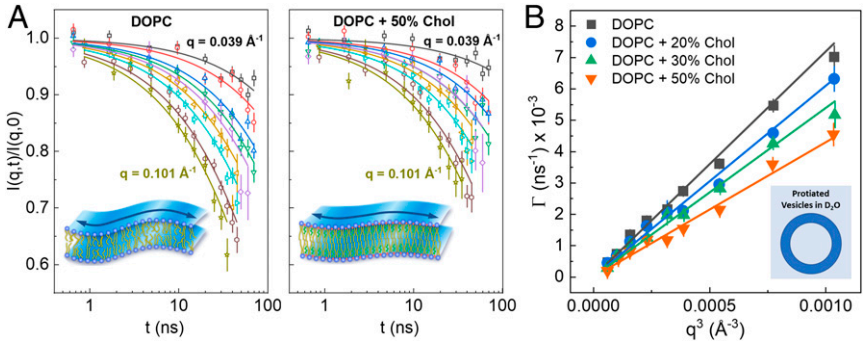

Fig. 2. NSE spectroscopy studies on DOPC–Chol vesicles indicate decrease in local fluctuation dynamics with increasing Chol content. (*A*) Intermediate scattering functions, $I(q,t)/I(q,0)$, of protiated DOPC bilayers with no Chol (*Left*) and 50 mol% Chol (*Right*) show clear slowdown in the measured dynamics in DOPC–Chol membranes. Solid lines are fits to the data using the Zilman–Granek model for membrane bending fluctuations (*SI Appendix*, Eq. **S8**). (*B*) q-dependence of the decay rates $\Gamma(q)$ for protiated DOPC–Chol vesicles in D_2O (*Inset*). The solid lines depicting linear fits according to Eq. **1** follow the classical q^3 behavior of bending undulations. A decrease in the slope of the solid lines with increasing Chol content indicates an increase in the effective bending modulus. Error bars represent ±1 SD.

Keeping in mind that $\Gamma_{\text{bend}}(q)$ is proportional to $\sqrt{1/\kappa}$, one can thus appreciate the large effect that the observed differences would have on the effective bending-rigidity moduli. It is also worth noting here that NSE is sensitive to internal dissipation mechanisms, as shown by Watson and Brown (41)—we will explore this later in *Discussion*.

Solid-State ^{2}H NMR Spectroscopy Shows Chol-Induced Reduction in Elastic Deformations in DOPC Bilayers. Solid-state ^{2}H NMR nuclear-spin-relaxation experiments (19, 43, 44) provide atomistically resolved information about collective membrane dynamics, such as elastic deformations of the acyl-chain region within the membrane (*SI Appendix*). Perturbation of the magnetization away from the equilibrium state allows for the observation of time-resolved magnetization recovery (Fig. 3*A* and *SI Appendix*, Fig. S7), leading to an experimentally measurable spin-lattice ($R_{1Z}^{(i)}$) relaxation rate for each deuterated segment (i). Relaxation rates in the limit of small-amplitude director fluctuations often follow a square-law dependence on the segmental order parameter, $S_{CD}^{(i)}$, as predicted by Brown (45), with a slope that is inversely related to the membrane stiffness (19). Following this model-free interpretation of spin-lattice relaxations, where the slope decreased with increasing Chol content, our measurements indicated unambiguous Chol-induced stiffening of DOPC bilayers, as shown in Fig. 3*B*. For quantitative estimates of κ, the viscoelastic constant $= 3k_BT\sqrt{\eta}/5\pi S_s^2\sqrt{2K^3}$, (where K is a single elastic constant, η is the bilayer viscosity coefficient, and S_s is the order parameter for slower motions) was directly obtained from the slope of the square law plots (46–48) (Fig. 3*B*). The values of κ were then calculated from the viscoelastic constant and the bilayer thickness $t = 2D_C$, such that $\kappa \approx Kt$. Notably, the calculated bending-rigidity moduli showed ~3.5-fold relative increase for DOPC–Chol membranes with 50 mol% Chol, i.e., $\kappa/\kappa_0 \sim 3.5$ (Fig. 4*A*), in excellent agreement with our NSE results. These results are also consistent with a recent report on protiated DOPC membranes using a relatively low-resolution proton NMR relaxation dispersion method (49).

Additionally, we note that the solid-state ^{2}H NMR studies of protiated DOPC–Chol mixtures introduced a deuterated POPC-d_{31} proxy lipid probe (10 mol%) to detect the properties of the host lipid bilayer. This was a reasonable alternative to using DOPC-d_{66} with perdeuterated chains, which posed a challenge to data interpretation due to the considerable overlap of the quadrupolar splittings from the two unsaturated acyl groups in DOPC. Control studies (*SI Appendix*, Fig. S8) showed that the use of 10 mol% POPC-d_{31} adequately sampled the structure and dynamics of the host POPC membrane. For instance, order parameters and relaxation rates were statistically indistinguishable from those of pure POPC-d_{31} multilamellar dispersions. More importantly, when 10 mol% POPC-d_{31} was incorporated in a

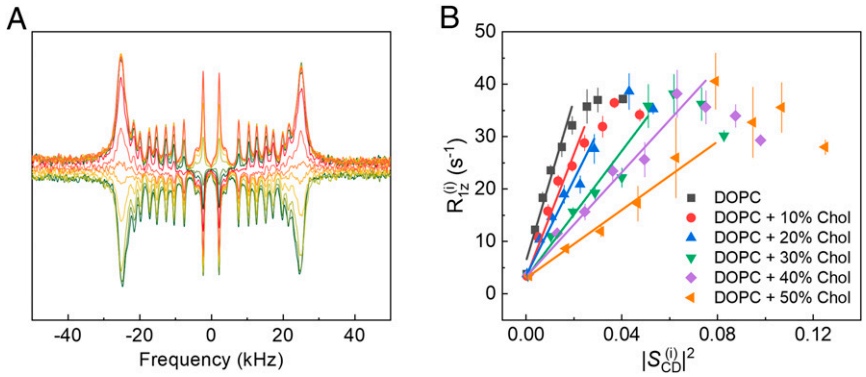

Fig. 3. The ^{2}H NMR relaxometry on multilamellar stacks of DOPC–Chol membranes indicates a decrease in membrane elasticity with higher Chol content. (*A*) Inversion recovery spectra of ^{2}H nuclear magnetization for DOPC multilamellar dispersion using 10 mol% POPC-d_{31} probe. (*B*) The ^{2}H NMR relaxometry measurements show primarily linear dependence of the relaxation rate $R_{1Z}^{(i)}$ on the squared-order parameters, $\left|S_{CD}^{(i)}\right|^2$. The decrease in the square law slopes indicates a reduction in DOPC bilayer elasticity with increasing Chol fraction. Error bars represent ±1 SD from the mean.

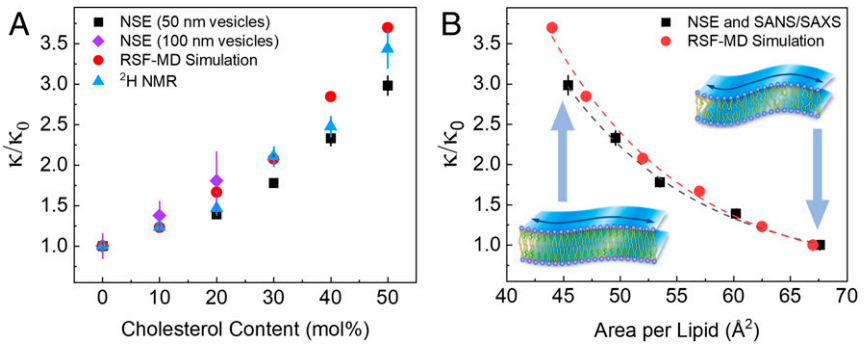

Fig. 4. NSE spectroscopy, ^{2}H NMR relaxometry, and MD simulations show almost identical increases in the bending modulus of DOPC membranes with increasing Chol. (*A*) Relative bending rigidity moduli (κ/κ_0) calculated from nanoscale bending fluctuations sampled by NSE spectroscopy, ^{2}H NMR relaxometry, and RSF analysis of MD simulations. All three techniques show up to an ~3-fold increase in DOPC–Chol membranes with Chol content approaching 50 mol%. κ_0 is the bending rigidity of DOPC membranes measured by the respective technique. (*B*) Plots of κ/κ_0 vs. the area per lipid show consistent trends between mechanical and structural parameters obtained from NSE and SAXS/SANS and from RSF-MD simulations. The results suggest that Chol-induced stiffening in DOPC membranes, on the length and time scales of NSE and MD, is driven by Chol inducing lipids to pack more closely. The dashed lines are a guide to the eye. Error bars represent ±1 SD from the mean.

host DOPC membrane, the resulting relaxation rates indicated a "softer" membrane environment relative to POPC (*SI Appendix*, Fig. S8), as expected from the known structural properties of POPC and DOPC bilayers (50, 51). We also note that solid-state ^{2}H NMR analysis (45, 52, 53) is based on the assumption that the time scales of distinct motional components are sufficiently different to distinguish them as either fast or slow motions, i.e., statistically independent with no cross-correlations. Only the segments that are not strongly coupled to the slow motions are considered in the analysis of the square-law plots. For lipid membranes like DOPC, the time scales of fast collective lipid motions may overlap with nematic-like director fluctuations, leading to nonlinear behavior of the square-law plot for higher parameters, i.e., closer to the polar head groups (Fig. 3*B*). We thus limit our current analysis to the segmental order parameters that show the typical square-law behavior of the relaxation rates.

Stiffening Effect of Chol on DOPC Membranes Quantified from Atomistic MD Simulations. Our MD simulations offered another means for studying membrane mechanics by analyzing the thermal fluctuations of a relatively flat membrane patch (54–57). Having validated the series of DOPC–Chol simulations with structural measurements, we examined the stiffening effect of Chol on bilayers in an expanded set of simulations with Chol content between 0 mol% and 50 mol%. The membrane bending rigidity was obtained from analyzing the local fluctuations in the lipid-splay degrees of freedom (27, 28)—that is, how the orientation of neighboring DOPC and Chol molecules varied with respect to one another over the course of the simulation trajectories. As shown elsewhere (27), this type of local RSF analysis has been effectively used to quantify the elastic properties of a wide range of membranes. Notably, the RSF approach closely resembles the NSE and solid-state ^{2}H NMR lipid membrane data. The three approaches access local membrane fluctuations over similar time scales and can thus be directly compared. For example, previous simulations of 1,2-dimyristoyl-*sn*-glycero-3-phosphocholine (DMPC) membranes at 30 °C reported an RSF value of $\kappa \approx 34.7 k_BT$, which is in excellent agreement with NSE studies of DMPC vesicles ($\kappa \approx 35 k_BT$) (31). Analogous simulations of DOPC membranes at 25 °C yielded $\kappa = (18.3 \pm 0.3) k_BT$ (28), a result in close agreement with the NSE results from the 100-nm-diameter DOPC vesicles. More importantly, the simulations clearly showed an increase in relative membrane bending rigidity with increasing Chol content (Fig. 4*A* and *SI Appendix*, Table S5), up to $\kappa/\kappa_0 \sim 3.5$ for DOPC–Chol membranes with 50 mol% Chol. Summarized in Fig. 4*A*, the results from simulated membranes agree with the relative bending moduli obtained experimentally by both NSE spectroscopy and solid-state ^{2}H NMR relaxometry, lending yet another piece of evidence for the strong stiffening effect of Chol on DOPC membranes over the length and time scales accessed by these three different techniques.

Mechanism of Chol Stiffening in DOPC Membranes Relates to the Increase in Bilayer Packing Density and Area Compressibility. To further investigate the mechanisms by which Chol affects local membrane mechanics, we hypothesized that the changes in κ observed by NSE and solid-state ^{2}H NMR are due to Chol inducing the lipids to pack more closely. To test this idea, we plotted the bilayer κ/κ_0 values against A_L and found that the relationship between bending rigidity and lipid packing was the same from the MD simulations and NSE experiments (Fig. 4*B*). This finding suggests that the primary mechanism by which Chol increases the stiffness of DOPC membranes is by reducing the average area per lipid. The simulations also provided insights into the compression-bending relationship and illustrated the role of chain unsaturation on the mechanical properties of DOPC–Chol membranes. The simulations were thus used to calculate the area-compressibility modulus in relation to the bending rigidity and the bilayer's p-p thickness. To this end, we used the polymer-brush model proposed by Evans and coworkers (32) to describe the coupling between the two leaflets in a lipid bilayer. The significance of the model is that it relates K_A to κ via the membrane mechanical thickness and a β parameter that represents the strength of coupling of the two leaflets; for lipid bilayers, $\beta = 24$. Interestingly, the model was shown to work well for single-component lipid bilayers, but not for unsaturated lipid membranes containing Chol, such as DOPC–Chol (23). However, recent studies by Doktorova et al. (28), using extensive simulations and data comparisons, showed that redefining the mechanical thickness of DOPC–Chol membranes by excluding the incompressible regions around the double bonds in contact with Chol restored the standard K_A vs. κ dependence predicted by the polymer-brush model. Here, we applied the same approach in the analysis of NSE data on tail-perdeuterated lipid membranes, as discussed below.

NSE Studies of Thickness Fluctuations Show that Chol Increases the Viscosity of DOPC Membranes. In addition to bending fluctuations, NSE experiments using tail-perdeuterated membranes (i.e., DOPC-d_{66} and Chol-d_{40}) in deuterated buffer give access to another collective dynamic mode in lipid membranes, namely, thickness fluctuations (58–60). Contrast matching the tail region of the bilayer to

the solvent amplifies head–head correlations in the scattering signal, facilitating studies of membrane-thickness fluctuations. Measurements of this mode are facilitated by NSE's ability to simultaneously access the length scales (on the order of the membrane thickness) and time scales (on the order of a few hundred nanoseconds) over which thickness fluctuations occur (30, 61). In such measurements, thickness fluctuations manifest themselves as enhanced dynamics that appear in addition to bending fluctuations, as shown in Fig. 5*A*. The dynamics are most pronounced at q values that correspond to the membrane thickness, as was recently corroborated in coarse-grained MD simulations (62). To fit the observed excess dynamics, we follow the recent approach of Nagao et al. (31), which enables the extraction of biophysical membrane parameters following the theoretical framework of Bingham et al. (63). In this approach, the thickness-fluctuation signal is given by:

$$\frac{\Gamma}{q^3} = \frac{\Gamma_{\text{bend}}}{q^3} + \frac{K_A k_B T}{\mu q_0^3 k_B T + 4\mu q_0 K_A A_L (q - q_0)^2}, \quad [2]$$

where q_0 is the peak q value obtained from SANS, μ is the in-plane membrane viscosity, and K_A is the area-compressibility modulus obtained from independent NSE measurements of the bending rigidity on fully protiated membrane analogs using the modified polymer-brush model proposed by Doktorova et al. (28) (*SI Appendix*, Table S4). Subsequently, Eq. **2** only assumes one fitting parameter; i.e., the membrane viscosity, μ. By applying this to NSE data on 100-nm DOPC-d_{66} vesicles with (0, 10, and 20) mol% Chol-d_{40}, we were able to quantify the effects of Chol on membrane viscosity, as shown in Fig. 5*B*.

Strikingly, the viscosity value obtained from NSE thickness-fluctuation studies of DOPC membranes [μ = (16.7 ± 1.1) nPa·s·m] is in excellent agreement with recent results [μ = (15.3 ± 3.4) nPa·s·m] from tracer experiments that probed both rotational and translational diffusion coefficients of membrane-linked particles (64). In comparison, membranes with (10 and 20) mol% Chol exhibited higher viscosity values, namely, 26.3 and 31.9 nPa·s·m, respectively (*SI Appendix*, Table S4). The correlated increase in membrane viscosity and bending rigidity is in line with the effect of Chol on local viscoelastic membrane properties and its molecular-level suppression of elastic fluctuations. This result was shown both in NSE studies of POPC membranes (29) and in solid-state ^{2}H NMR experiments of DMPC-d_{54} membranes (19, 48).

Discussion

NSE and solid-state ^{2}H NMR experiments, coupled with RSF MD simulations—all of which access comparable length and time scales—yield similar trends of increasingly stiffer DOPC bilayers with increasing Chol content (Fig. 4*A*). The observed changes in membrane mechanics are commensurate with Chol-induced structural changes in DOPC membranes obtained from solid-state ^{2}H NMR lineshape analysis, as well as SAXS/SANS and spin-label ESR measurements. These changes are characterized by increased molecular packing and membrane thickness, in agreement with previous studies of phosphatidylcholine–Chol membranes (36). The synergistic changes in the structural and dynamical membrane properties indicate that Chol affects unsaturated DOPC membranes through a lipid-packing mechanism similar to what has been seen in saturated lipid membranes (23). The current observations reaffirm structure–property relations in lipid membranes (65, 66) and show that, with a modified mechanical membrane thickness, the polymer-brush model holds for a wide range of membrane types, including unsaturated lipid membranes enriched with Chol.

Chol Increases Bending Rigidity of Unsaturated Lipid Bilayers. Chol is known to increase the bending rigidity of saturated lipid membranes (23, 24) through increased packing density and bilayer thickness (35). Yet studies of unsaturated lipids, such as DOPC, have shown surprisingly different trends. Despite evidence that Chol exhibits similar structural effects on unsaturated lipid membranes, it has been reported to have no influence on the membrane bending rigidity (24, 67). Interestingly, elasticity studies of DOPC–Chol membranes show a strong Chol-dependence of the area-compressibility modulus, specifically, up to an ∼3-fold increase at a Chol content of 50 mol% (68). This unintuitive behavior observed in DOPC–Chol membranes challenges our general understanding of the coupling between area compressibility and bending rigidity. For example, based on deformation models of elastic thin sheets (32), κ is proportional to the area-compressibility modulus, K_A, such that $\kappa = K_A t_m^2/\beta$, where t_m is the mechanical (or deformable) membrane thickness and β is a constant that describes interleaflet coupling [i.e., β = 12 for fully coupled leaflets, β = 48 for completely uncoupled leaflets, and β = 24 for fluid lipid membranes, according to the polymer-brush model (32)]. To explain the contradiction in the K_A and κ trends of DOPC–Chol membranes, it has been suggested that the polymer-brush model does not hold for Chol-containing unsaturated lipid membranes (23). Instead, a different relation between K_A and κ was hypothesized, albeit only applicable to DOPC membranes with 50 mol% Chol, where t_m is replaced by the length of the sterol ring in the above-mentioned expression. In contrast, MD simulations by Doktorova et al. (28) showed that, with a modified assignment of the mechanical

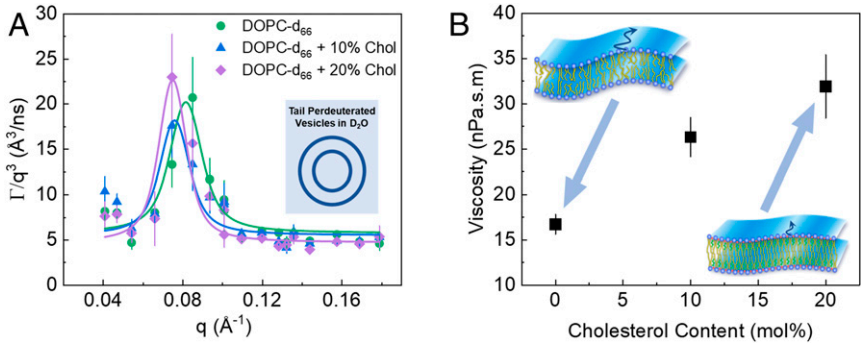

Fig. 5. NSE studies on selectively deuterated DOPC–Chol membranes show Chol-induced increase in membrane viscosity. (*A*) NSE relaxation rates measured by using tail-perdeuterated DOPC–Chol membranes in deuterated buffer solution, with a neutron contrast scheme depicted in the *Inset*. In addition to the q^3 signal from bending relaxation, there are additional dynamics attributed to thickness fluctuations, which are adequately fitted by using Eq. **2**. (*B*) Fits of the thickness fluctuations yield increasing membrane viscosity with increasing mol% Chol, emphasizing the effect of Chol on local lipid dynamics. Error bars represent ±1 SD from the mean.

membrane thickness, the polymer-brush model is applicable to a wide range of membrane types, including unsaturated lipid membranes enriched with Chol. Following this approach, our measurements on DOPC–Chol bilayers revealed consistent effects of Chol on elastic membrane properties—i.e., bending rigidity and area compressibility—in accord with current understanding of membrane structure–property relations.

Length- and Time-Scale Dependence of Bending Rigidity of Lipid Membranes. The current observations of mesoscale Chol-induced stiffening in DOPC–Chol membranes are in striking contrast with conclusions from previous studies of Chol-enriched unsaturated lipid bilayers that used diffuse X-ray scattering from multilamellar planar membranes (67) or micropipette aspiration and electrodeformation of micrometer-sized giant unilamellar vesicles (GUVs) (24). Unlike the present findings, those studies reported almost no effect of Chol on the bending rigidity of DOPC–Chol membranes over the same range of Chol concentrations, as studied in our work. Here, we propose that these discrepancies can be explained by differences in the accessible length and time scales of the different measurement techniques. For example, membrane elastic properties from diffuse X-ray scattering of multimembrane stacks are extracted by using the Helfrich theory (69), where the diffuse scattering signal is treated as a signature of long-range intermembrane interactions that result in long-wavelength fluctuations (70). More recent X-ray diffusivity experiments (23) have accessed smaller length scales, but still sampled membrane dynamics over acquisition times on the order of hours to calculate the fluctuation amplitude. Correspondingly, measurements of GUVs using micropipette aspiration or electrodeformation were primarily based on the analysis of micrometer-scale shape fluctuations taking place over millisecond time scales. These length and time scales are orders of magnitude larger than those accessed by NSE, solid-state ^{2}H NMR, and RSF-MD simulations used in this study, which probe the emergent bending fluctuations over local lipid environments. For instance, the q-range accessed by NSE experiments corresponds to length scales of ∼100 Å and is measured over time scales of subnanoseconds to 100 ns, emphasizing the local and rapid nature of the probed bending fluctuations. Similarly, solid-state ^{2}H NMR and RSF-MD analyses are based on fluctuations in the local splay of lipid directors, as has been described (44, 45). The differences in emergent bending fluctuations measured over different length and time scales present an intriguing notion of hierarchical manifestations of membrane dynamics, which could significantly impact our understanding of how biological processes on the molecular level affect macroscale properties.

To investigate this proposal further, we performed spatial and temporal analysis of simulation trajectories on the DOPC–Chol membranes, as well as a stearoyl sphingomyelin (SSM) membrane with 30 mol% Chol, a well-studied lipid system (24). Specifically, we investigated the length- and time-scale dependence of the bending modulus by quantifying how the splay angle between pairs of lipids changes as a function of distance between the two lipids and over time (*SI Appendix*, Fig. S9*A*). The results show that, as Chol concentration increases, the orientational order in the DOPC bilayer increases; however, even for the highest Chol content (50 mol%), DOPC membranes show less orientational order and more spatial variations compared to the SSM bilayer with 30 mol% Chol. As the lipid-splay degrees of freedom directly relate to the bending modulus in the simulations, this analysis suggests that bending-rigidity measurements that sample different length scales would yield similar results for SSM–Chol membranes, but not for DOPC–Chol membranes. In addition, we found that correlations in the lipid splay for the SSM–Chol bilayer persist over longer time scales compared to DOPC–Chol bilayers (*SI Appendix*, Fig. S9*B*). This could explain the differences in experimental measurements of bending rigidity over different time scales.

Membrane Mechanics on the Mesoscale Revealed by an Integrated Approach. The remarkable agreement between the three local measurement modalities used in this study—and the deviation from micrometer-scale observations of membrane bending fluctuations—indicates the existence of a hierarchical energy landscape in Chol-containing lipid membranes. A plausible explanation for these differences entails the time scales over which the bending dynamics manifest, as illustrated in a recent MD-simulation approach based on the enhanced sampling of the free energy of membrane deformations (71). The concept of sampling, or scale-dependent dynamics in lipid membranes, was theoretically introduced in the early work by Seifert and Langer (42) that considered internal membrane dissipation, such as monolayer density fluctuations (or area compressibility) and internal membrane dissipation (or viscous modes), together with bending dynamics. Within this model, the dispersion relationship of bending fluctuations depends on the length and time scales over which molecular redistribution within monolayers can take place. Measurements of long fluctuation wavelengths, or over long times, sample the bending fluctuations that occur at relaxed lipid-monolayer densities. At shorter wavelengths, or for short relaxation times, the lipid molecules cannot redistribute fast enough, resulting in an increase in the effective bending rigidity. This mechanism may explain the current results, namely, that Chol impacts molecular redistribution within the membrane, as well as contributing to the observed bending dynamics. Analogous observations were reported in recent NSE studies of POPC–Chol membranes (72). Here, we expect a similar mechanism for the slowdown in bending relaxations observed in both the NMR experiments and MD simulations. Our explanation is reinforced by the findings of increasing membrane viscosity with increasing Chol content, supporting the notion that Chol strongly influences local lipid reorganization, resulting in a slowdown of the local bending dynamics. Such a mechanism can influence membrane proteins or other biomolecules, necessitating direct experimental observations, like those reported here, to understand cellular function on relevant length and time scales.

Further support for the above interpretation of the effect of Chol on membrane bending rigidity comes from the observed increase in membrane area compressibility K_A (*SI Appendix*, Table S4), which agrees well with measurements by Evans et al. (68). In their studies, the authors reported that the area-compressibility modulus of unsaturated DOPC–Chol membranes exhibited a strong dependence on Chol content, with up to ∼3-fold increase in K_A at 50 mol% Chol, compared to pure DOPC membranes. This observation lends additional validity to the notion that the stiffening mechanism of Chol in DOPC membranes is driven by Chol-mediated lipid packing and its effect on lipid arrangements and local monolayer densities. Our results point to the possibility that membrane dynamics sampled over different scales could result in different emergent membrane properties. On the length and time scales probed in this work, Chol-induced mechanics in DOPC–Chol membranes follow the conventional structure–property relations dictated by the polymer-brush model, in which the membrane bending rigidity is primarily governed by increased lipid packing and area-compressibility modulus.

The current study clarifies a long-debated mechanical picture of Chol and its function in unsaturated lipid membranes. We have presented data from three complementary techniques (NSE spectroscopy, solid-state ^{2}H NMR spectroscopy, and RSF-MD simulations) to evaluate the effects of Chol on the local mechanical properties of DOPC membranes as a prototype for (poly)unsaturated lipid bilayers (73). All three techniques showed a monotonic increase in the bending rigidity of DOPC

bilayers with increasing levels of Chol. Elastic membrane parameters determined from NSE and solid-state ^{2}H NMR measurements yielded almost identical trends, which agreed with corresponding parameters obtained from RSF-MD simulations—an important outcome, given that the three different methods sample the same mesoscale fluctuation modes in evaluating membrane mechanics. All methods indicate a strong dependence of the bending rigidity on Chol content in DOPC membranes, with an ∼3-fold increase in membrane rigidity at 50 mol % Chol, compared to Chol-free DOPC membranes. This increase in bending rigidity is accompanied by an increase in the area-compressibility modulus and packing density, measured independently by SAXS/SANS, solid-state ^{2}H NMR relaxometry, and ESR experiments and corroborated by MD simulations.

Biophysical Significance. The observations of local stiffening due to the presence of Chol in unsaturated DOPC membranes have important biological implications. Given the abundance of Chol in cell membranes and the wide variety of lipids they host, the current results encourage a reassessment of Chol's effect on the local elastic and viscoelastic properties of membranes with different lipid compositions. Further extrapolation to membranes with different levels of lipid (poly)unsaturation or multicomponent membranes, under various solution conditions, will shed light on possible differences in the mechanical response of lipid membranes in relevant biological environments, as in the case of asymmetric lipid bilayers or domain-forming bilayers. Such investigations will be key to understanding the role of local membrane mechanics in vital biological functions that occur on mesoscopic length and time scales, including viral budding and lipid–protein interactions. For instance, how Chol affects membrane budding in the maturation of viruses, such as HIV and coronavirus, remains an urgent biological question with profound societal, economic, and scientific impact.

Materials and Methods

Sample Preparation. Protiated phospholipids and Chol (ovine wool, >98%) were purchased from Avanti Polar Lipids as dry powders and used as supplied. Ultrapure H_2O was obtained from a High-Q purification system. D_2O (99.9%) was purchased from Cambridge Isotope Laboratories. Perdeuterated DOPC-d_{66} and Chol-d_{40} were synthesized according to the protocol outlined in *SI Appendix*. Lipid membranes were prepared in the form of large unilamellar vesicles (LUVs) for NSE, SANS, and SAXS experiments; multilamellar vesicles for ESR experiments; and multilamellar stacks for NMR experiments. All samples were prepared by first dissolving lipids in chloroform or methanol:hexane solutions, then completely evaporating the solvent (overnight vacuum drying), followed by hydration with buffer and applying five freeze/thaw cycles to ensure sample homogeneity. For LUV suspensions, an additional extrusion step was performed. More details are provided in *SI Appendix*.

SAXS/SANS. SAXS measurements were done by using a Rigaku BioSAXS-2000 system (Rigaku Americas) with a HF007 copper rotating anode, a Pilatus 100K two-dimensional (2D) detector, and an automatic sample changer. SAXS data were collected at a fixed sample-to-detector distance calibrated by using a silver behenate standard, with a typical data-collection time of 3 h. The one-dimensional (1D) scattering intensity was obtained by radial averaging of the corrected 2D detector images, after background subtraction, using the Rigaku SAXSLab software. SANS experiments were performed at the NGB-30m SANS instrument at the National Institute of Standards and Technology (NIST) Center for Neutron Research (NCNR). SANS data were collected on LUV suspensions over a q range of ∼0.001 to 0.5 Å^{-1}. Similar to SAXS, the 1D SANS signals were obtained from circular averaging of the 2D scattering signals after correcting for resolution, empty cell scattering, and background. The 1D SAXS/SANS data were analyzed by using the theoretical framework described in *SI Appendix*.

ESR. ESR measurements were performed on multilamellar vesicles of DOPC–Chol membranes doped with 1-palmitoyl-2-stearoyl-(16-doxyl)-*sn*-glycero-3-phosphocholine, a lipid spin probe labeled with a nitroxide functional group at the 16th carbon position. ESR spectra were recorded on a Bruker EleXsys-II E500 CW ESR spectrometer operating at X-band frequency (9.4 GHz). The spectrometer settings for all samples were as follows: center field = 3,362.9 G, sweep width = 100 G, microwave power = 0.3170 mW, modulation frequency = 100 kHz, modulation amplitude = 0.8 G, and resolution (points) = 1,024. Reported spectra are the average of 4 to 16 scans, depending on the signal intensity. Normalized spectra, following a standard protocol outlined in *SI Appendix*, were used for the calculation of the order parameter of DOPC–Chol membranes.

NSE Spectroscopy. NSE experiments were conducted on the NSE spectrometer at NCNR and on the NSE spectrometer at the Spallation Neutron Source (SNS) at Oak Ridge National Laboratory (ORNL). Measurements were performed on 50 mg/mL LUV suspensions of protiated and tail-perdeuterated DOPC–Chol membranes in D_2O buffer at 25 °C. Fully protiated membranes were used for measurements of bending fluctuations, whereas tail-perdeuterated membranes (prepared with DOPC-d_{66} and Chol-d_{40}) were used for measurements of thickness fluctuations. Experiments on the NCNR-NSE spectrometer were performed over a q range of (0.04 to 0.1) Å^{-1} for protiated vesicles and (0.04 to 0.18) Å^{-1} for tail-perdeuterated vesicles. Experiments at the SNS-NSE spectrometer were performed over a q range of (0.05 to 0.15) Å^{-1}. In both cases, the instrument resolution and the D_2O buffer were measured under the same configurations for data reduction and normalization. Experiments at the SNS-NSE spectrometer were limited to DOPC vesicles with 20 mol% Chol and yielded statistically indistinguishable results compared to NCNR-NSE data.

Solid-State ^{2}H NMR Spectroscopy. Experimental ^{2}H NMR spectra were acquired with a Bruker AMX-500 spectrometer (11.78 T magnetic field strength, ^{2}H frequency 76.77 MHz). Powder-type spectra for the multilamellar lipid dispersions were recorded with a phase-cycled, quadrupolar echo sequence [i.e., $(\pi/2)_x - d_6 - (\pi/2)_y - d_7 -$ acquire]. A home-built solid-state probe with an 8-mm-diameter coil and high-voltage capacitors (Polyflon) was used with a Bruker radiofrequency amplifier to generate 5-μs 90° pulses. Powder-type spectra (Pake patterns) were obtained by Fourier transformation of quadrupolar echoes, starting at the echo top with a fast Fourier transform algorithm using an in-house MATLAB routine. The ^{2}H NMR spectra were numerically inverted by using the de-Pakeing method to obtain equilibrium spectra corresponding to the $\theta = 0°$ bilayer orientation relative to the external magnetic field. Spin-lattice relaxation times were measured by using an inversion recovery pulse sequence, i.e., $(\pi)_x - \tau - (\pi/2)_x - d_6 - (\pi/2)_y - d_7 -$ acquire. Partially relaxed spectra were recorded at 14 variable delays (τ), following the inverting π pulse. The spin-lattice relaxation rates for each resolved peak were obtained by nonlinear regression fitting (*SI Appendix*).

MD Simulations. Detailed information about the setup of the all-atom systems, their simulation and analysis can be found in the *SI Appendix*.

Data Availability. Experimental data can be accessed at Virginia Tech's Data Repository (VTechData; DOI: 10.7294/v8w6-7760).

ACKNOWLEDGMENTS. We thank E. G. Kelley for discussions and assistance in SANS and NSE data collection. We also acknowledge the use of neutron-scattering facilities at NIST and ORNL. R.A. was supported by faculty startup funds from the state of Virginia and the Clifford G. Shull Fellowship program sponsored by the Neutron Sciences Directorate at ORNL. F.N.B. received partial support from NIH Grant R01GM120642, and F.A.H. was supported by NSF Grant MCB-1817929. G.K. was supported by the 1923 Fund. J.K. is supported through the Scientific User Facilities Division of the Department of Energy (DOE) Office of Science, sponsored by the Basic Energy Science (BES) Program, DOE Office of Science, under Contract DEAC05-00OR22725. M.N. was supported by Cooperative Agreement 70NANB15H259 from NIST, U.S. Department of Commerce. M.F.B. was supported by NIH Grant R01EY026041 and NSF Grants MCB-1817862 and CHE-1904125. M.D. was supported by NIH Grant 1F32GM134704-01. Access to the NIST SANS and NSE beamlines was provided by the Center for High Resolution Neutron Scattering, a partnership between the NIST and the NSF under Agreement DMR-1508249. Research conducted at ORNL's SNS was sponsored by the Scientific User Facilities Division, Office of BES, US DOE. ORNL is managed by UT-Battelle, LLC under US DOE Contract DE-AC05-00OR22725. ACERT is supported by NIH Grants P41GM103521 and R01GM123779. This work benefited from the use of the SasView application, originally developed under NSF Award DMR-0520547. Any mention of commercial products within NIST web pages is for information only; it does not imply recommendation or endorsement by NIST.

1. O. G. Mouritsen, M. J. Zuckermann, What's so special about cholesterol? *Lipids* **39**, 1101–1113 (2004).
2. G. van Meer, D. R. Voelker, G. W. Feigenson, Membrane lipids: Where they are and how they behave. *Nat. Rev. Mol. Cell Biol.* **9**, 112–124 (2008).
3. F. R. Maxfield, G. van Meer, Cholesterol, the central lipid of mammalian cells. *Curr. Opin. Cell Biol.* **22**, 422–429 (2010).
4. E. Corvera, O. G. Mouritsen, M. A. Singer, M. J. Zuckermann, The permeability and the effect of acyl-chain length for phospholipid bilayers containing cholesterol: Theory and experiment. *Biochim. Biophys. Acta* **1107**, 261–270 (1992).
5. F. J. M. de Meyer, J. M. Rodgers, T. F. Willems, B. Smit, Molecular simulation of the effect of cholesterol on lipid-mediated protein-protein interactions. *Biophys. J.* **99**, 3629–3638 (2010).
6. F. Cornelius, Modulation of Na,K-ATPase and Na-ATPase activity by phospholipids and cholesterol. I. Steady-state kinetics. *Biochemistry* **40**, 8842–8851 (2001).
7. J. Bernardino de la Serna, J. Perez-Gil, A. C. Simonsen, L. A. Bagatolli, Cholesterol rules: Direct observation of the coexistence of two fluid phases in native pulmonary surfactant membranes at physiological temperatures. *J. Biol. Chem.* **279**, 40715–40722 (2004).
8. Y. Deng, Z. A. Almsherqi, M. M. L. Ng, S. D. Kohlwein, Do viruses subvert cholesterol homeostasis to induce host cubic membranes? *Trends Cell Biol.* **20**, 371–379 (2010).
9. X. Sun, G. R. Whittaker, Role for influenza virus envelope cholesterol in virus entry and infection. *J. Virol.* **77**, 12543–12551 (2003).
10. V. R. Prasad, M. I. Bukrinsky, New clues to understanding HIV nonprogressors: Low cholesterol blocks HIV trans infection. *MBio* **5**, e01396-14 (2014).
11. G. Meher, S. Bhattacharjya, H. Chakraborty, Membrane cholesterol modulates oligomeric status and peptide-membrane interaction of severe acute respiratory syndrome coronavirus fusion peptide. *J. Phys. Chem. B* **123**, 10654–10662 (2019).
12. K. Matsuzaki, K. Sugishita, N. Fujii, K. Miyajima, Molecular basis for membrane selectivity of an antimicrobial peptide, magainin 2. *Biochemistry* **34**, 3423–3429 (1995).
13. A. Khondker *et al*., Membrane cholesterol reduces polymyxin B nephrotoxicity in renal membrane analogs. *Biophys. J.* **113**, 2016–2028 (2017).
14. A. J. McHenry, M. F. M. Sciacca, J. R. Brender, A. Ramamoorthy, Does cholesterol suppress the antimicrobial peptide induced disruption of lipid raft containing membranes? *Biochim. Biophys. Acta* **1818**, 3019–3024 (2012).
15. E. Endress, H. Heller, H. Casalta, M. F. Brown, T. M. Bayerl, Anisotropic motion and molecular dynamics of cholesterol, lanosterol, and ergosterol in lecithin bilayers studied by quasi-elastic neutron scattering. *Biochemistry* **41**, 13078–13086 (2002).
16. N. Khatibzadeh, A. A. Spector, W. E. Brownell, B. Anvari, Effects of plasma membrane cholesterol level and cytoskeleton F-actin on cell protrusion mechanics. *PLoS One* **8**, e57147 (2013).
17. I. Titushkin, M. Cho, Distinct membrane mechanical properties of human mesenchymal stem cells determined using laser optical tweezers. *Biophys. J.* **90**, 2582–2591 (2006).
18. R. Dimova, Recent developments in the field of bending rigidity measurements on membranes. *Adv. Colloid Interface Sci.* **208**, 225–234 (2014).
19. G. V. Martinez, E. M. Dykstra, S. Lope-Piedrafita, C. Job, M. F. Brown, NMR elastometry of fluid membranes in the mesoscopic regime. *Phys. Rev. E* **66**, 050902 (2002).
20. W. Helfrich, Elastic properties of lipid bilayers: Theory and possible experiments. *Z. Naturforsch. C* **28**, 693–703 (1973).
21. P. Bassereau, B. Sorre, A. Lévy, Bending lipid membranes: Experiments after W. Helfrich's model. *Adv. Colloid Interface Sci.* **208**, 47–57 (2014).
22. D. Boal, *Mechanics of the Cell* (Cambridge University Press, Cambridge, UK, ed. 2, 2002).
23. J. Pan, S. Tristram-Nagle, J. F. Nagle, Effect of cholesterol on structural and mechanical properties of membranes depends on lipid chain saturation. *Phys. Rev. E* **80**, 021931 (2009).
24. R. S. Gracià, N. Bezlyepkina, R. L. Knorr, R. Lipowsky, R. Dimova, Effect of cholesterol on the rigidity of saturated and unsaturated membranes: Fluctuation and electrodeformation analysis of giant vesicles. *Soft Matter* **6**, 1472–1482 (2010).
25. B. J. Reynwar *et al*., Aggregation and vesiculation of membrane proteins by curvature-mediated interactions. *Nature* **447**, 461–464 (2007).
26. M. F. Brown, Soft matter in lipid-protein interactions. *Annu. Rev. Biophys.* **46**, 379–410 (2017).
27. M. Doktorova, D. Harries, G. Khelashvili, Determination of bending rigidity and tilt modulus of lipid membranes from real-space fluctuation analysis of molecular dynamics simulations. *Phys. Chem. Chem. Phys.* **19**, 16806–16818 (2017).
28. M. Doktorova, M. V. LeVine, G. Khelashvili, H. Weinstein, A new computational method for membrane compressibility: Bilayer mechanical thickness revisited. *Biophys. J.* **116**, 487–502 (2019).
29. L. R. Arriaga *et al*., Stiffening effect of cholesterol on disordered lipid phases: A combined neutron spin echo + dynamic light scattering analysis of the bending elasticity of large unilamellar vesicles. *Biophys. J.* **96**, 3629–3637 (2009).
30. A. C. Woodka, P. D. Butler, L. Porcar, B. Farago, M. Nagao, Lipid bilayers and membrane dynamics: Insight into thickness fluctuations. *Phys. Rev. Lett.* **109**, 058102 (2012).
31. M. Nagao, E. G. Kelley, R. Ashkar, R. Bradbury, P. D. Butler, Probing elastic and viscous properties of phospholipid bilayers using neutron spin echo spectroscopy. *J. Phys. Chem. Lett.* **8**, 4679–4684 (2017).
32. W. Rawicz, K. C. Olbrich, T. McIntosh, D. Needham, E. Evans, Effect of chain length and unsaturation on elasticity of lipid bilayers. *Biophys. J.* **79**, 328–339 (2000).
33. M. F. Brown, J. Seelig, Influence of cholesterol on the polar region of phosphatidylcholine and phosphatidylethanolamine bilayers. *Biochemistry* **17**, 381–384 (1978).
34. M. Alwarawrah, J. Dai, J. Huang, A molecular view of the cholesterol condensing effect in DOPC lipid bilayers. *J. Phys. Chem. B* **114**, 7516–7523 (2010).
35. W.-C. Hung, M.-T. Lee, F.-Y. Chen, H. W. Huang, The condensing effect of cholesterol in lipid bilayers. *Biophys. J.* **92**, 3960–3967 (2007).
36. N. Kučerka, J. Pencer, M. P. Nieh, J. Katsaras, Influence of cholesterol on the bilayer properties of monounsaturated phosphatidylcholine unilamellar vesicles. *Eur. Phys. J. E* **23**, 247–254 (2007).
37. M. Bloom, J. H. Davis, A. L. Mackay, Direct determination of the oriented sample NMR spectrum from the powder spectrum for systems with local axial symmetry. *Chem. Phys. Lett.* **80**, 198–202 (1981).
38. E. Sternin, M. Bloom, A. L. Mackay, De-pake-ing of NMR spectra. *J. Magn. Reson. (1969)* **55**, 274–282 (1983).
39. H. I. Petrache, S. W. Dodd, M. F. Brown, Area per lipid and acyl length distributions in fluid phosphatidylcholines determined by ^{2}H NMR spectroscopy. *Biophys. J.* **79**, 3172–3192 (2000).
40. A. G. Zilman, R. Granek, Undulations and dynamic structure factor of membranes. *Phys. Rev. Lett.* **77**, 4788–4791 (1996).
41. M. C. Watson, F. L. Brown, Interpreting membrane scattering experiments at the mesoscale: The contribution of dissipation within the bilayer. *Biophys. J.* **98**, L9–L11 (2010).
42. U. Seifert, S. A. Langer, Viscous modes of fluid bilayer membranes. *Europhys. Lett.* **23**, 71–76 (1993).
43. M. F. Brown, "Membrane structure and dynamics studied with NMR spectroscopy" in *Biological Membranes: A Molecular Perspective from Computation and Experiment*, K. M. Merz, B. Roux, Eds. (Birkhäuser Boston, Boston, MA, 1996), pp. 175–252.
44. T. R. Molugu, S. Lee, M. F. Brown, Concepts and methods of solid-state NMR spectroscopy applied to biomembranes. *Chem. Rev.* **117**, 12087–12132 (2017).
45. M. F. Brown, Theory of spin-lattice relaxation in lipid bilayers and biological membranes. ^{2}H and ^{14}N quadrupolar relaxation. *J. Chem. Phys.* **77**, 1576–1599 (1982).
46. L. Movileanu, D. Popescu, S. Ion, A. I. Popescu, Transbilayer pores induced by thickness fluctuations. *Bull. Math. Biol.* **68**, 1231–1255 (2006).
47. A. A. Nevzorov, M. F. Brown, Dynamics of lipid bilayers from comparative analysis of ^{2}H and ^{13}C nuclear magnetic resonance relaxation data as a function of frequency and temperature. *J. Chem. Phys.* **107**, 10288–10310 (1997).
48. T. R. Molugu, M. F. Brown, Cholesterol-induced suppression of membrane elastic fluctuations at the atomistic level. *Chem. Phys. Lipids* **199**, 39–51 (2016).
49. C. C. Fraenza, C. J. Meledandri, E. Anoardo, D. F. Brougham, The effect of cholesterol on membrane dynamics on different timescales in lipid bilayers from fast field-cycling NMR relaxometry studies of unilamellar vesicles. *ChemPhysChem* **15**, 425–435 (2014).
50. N. Kučerka *et al*., Areas of monounsaturated diacylphosphatidylcholines. *Biophys. J.* **97**, 1926–1932 (2009).
51. N. Kučerka, M.-P. Nieh, J. Katsaras, Fluid phase lipid areas and bilayer thicknesses of commonly used phosphatidylcholines as a function of temperature. *Biochim. Biophys. Acta* **1808**, 2761–2771 (2011).
52. R. L. Thurmond, G. Lindblom, "NMR studies of membrane lipid properties" in *Current Topics in Membranes*, R. M. Epand, Ed. (Academic Press, San Diego, CA, 1997), Vol. 44, pp. 103–166.
53. M. F. Brown, Theory of spin-lattice relaxation in lipid bilayers and biological membranes. Dipolar relaxation. *J. Chem. Phys.* **80**, 2808–2831 (1984).
54. E. R. May, A. Narang, D. I. Kopelevich, Role of molecular tilt in thermal fluctuations of lipid membranes. *Phys. Rev. E* **76**, 021913 (2007).
55. P. Tarazona, E. Chacón, F. Bresme, Thermal fluctuations and bending rigidity of bilayer membranes. *J. Chem. Phys.* **139**, 094902 (2013).
56. M. C. Watson, E. S. Penev, P. M. Welch, F. L. H. Brown, Thermal fluctuations in shape, thickness, and molecular orientation in lipid bilayers. *J. Chem. Phys.* **135**, 244701 (2011).
57. R. M. Venable, F. L. H. Brown, R. W. Pastor, Mechanical properties of lipid bilayers from molecular dynamics simulation. *Chem. Phys. Lipids* **192**, 60–74 (2015).
58. S. B. Hladky, D. W. Gruen, Thickness fluctuations in black lipid membranes. *Biophys. J.* **38**, 251–258 (1982).
59. H. W. Huang, Deformation free energy of bilayer membrane and its effect on gramicidin channel lifetime. *Biophys. J.* **50**, 1061–1070 (1986).
60. E. Lindahl, O. Edholm, Mesoscopic undulations and thickness fluctuations in lipid bilayers from molecular dynamics simulations. *Biophys. J.* **79**, 426–433 (2000).
61. R. Ashkar *et al*., Tuning membrane thickness fluctuations in model lipid bilayers. *Biophys. J.* **109**, 106–112 (2015).

62. J. Y. Carrillo, J. Katsaras, B. G. Sumpter, R. Ashkar, A computational approach for modeling neutron scattering data from lipid bilayers. *J. Chem. Theory Comput.* **13**, 916–925 (2017).
63. R. J. Bingham, S. W. Smye, P. D. Olmsted, Dynamics of an asymmetric bilayer lipid membrane in a viscous solvent. *Europhys. Lett.* **111**, 18004 (2015).
64. T. T. Hormel, S. Q. Kurihara, M. K. Brennan, M. C. Wozniak, R. Parthasarathy, Measuring lipid membrane viscosity using rotational and translational probe diffusion. *Phys. Rev. Lett.* **112**, 188101 (2014).
65. J. F. Nagle, Introductory lecture: Basic quantities in model biomembranes. *Faraday Discuss.* **161**, 11–29, discussion 113–150 (2013).
66. M. M. Terzi, M. F. Ergüder, M. Deserno, A consistent quadratic curvature-tilt theory for fluid lipid membranes. *J. Chem. Phys.* **151**, 164108 (2019).
67. J. Pan, T. T. Mills, S. Tristram-Nagle, J. F. Nagle, Cholesterol perturbs lipid bilayers nonuniversally. *Phys. Rev. Lett.* **100**, 198103 (2008).
68. E. Evans, W. Rawicz, B. A. Smith, Back to the future: Mechanics and thermodynamics of lipid biomembranes. *Faraday Discuss.* **161**, 591–611 (2013).
69. W. Helfrich, Steric interaction of fluid membranes in multilayer systems. *Z. Naturforsch.* **33**, 305–315 (1978).
70. C. R. Safinya *et al.*, Steric interactions in a model multimembrane system: A synchrotron X-ray study. *Phys. Rev. Lett.* **57**, 2718–2721 (1986).
71. G. Fiorin, F. Marinelli, J. D. Faraldo-Gómez, Direct derivation of free energies of membrane deformation and other solvent density variations from enhanced sampling molecular dynamics. *J. Comput. Chem.* **41**, 449–459 (2020).
72. L. R. Arriaga *et al.*, Dissipative curvature fluctuations in bilayer vesicles: Coexistence of pure-bending and hybrid curvature-compression modes. *Eur. Phys. J. E* **31**, 105–113 (2010).
73. A. Salmon, S. W. Dodd, G. D. Williams, J. M. Beach, M. F. Brown, Configurational statistics of acyl chains in polyunsaturated lipid bilayers from deuterium NMR. *J. Am. Chem. Soc.* **109**, 2600–2609 (1987).